Report

SOURCE DATA | TRANSPARENT PROCESS | OPEN ACCESS

EMBO reports

Insert L1 is a central hub for allosteric regulation of USP1 activity

Shreya Dharadhar, Willem J van Dijk, Serge Scheffers, Alexander Fish & Titia K Sixma*

Abstract

During DNA replication, the deubiquitinating enzyme USP1 limits the recruitment of translesion polymerases by removing ubiquitin marks from PCNA to allow specific regulation of the translesion synthesis (TLS) pathway. USP1 activity depends on an allosteric activator, UAF1, and this is tightly controlled. In comparison to paralogs USP12 and USP46, USP1 contains three defined inserts and lacks the second WDR20-mediated activation step. Here we show how inserts L1 and L3 together limit intrinsic USP1 activity and how this is relieved by UAF1. Intriguingly, insert L1 also conveys substrate-dependent increase in USP1 activity through DNA and PCNA interactions, in a process that is independent of UAF1-mediated activation. This study establishes insert L1 as an important regulatory hub within USP1 necessary for both substrate-mediated activity enhancement and allosteric activation upon UAF1 binding.

Keywords allostery; deubiquitinating enzyme; enzyme activity; quantitative kinetic modelling; translesion synthesis

Subject Categories DNA Replication, Recombination & Repair; Post-translational Modifications & Proteolysis

DOI 10.15252/embr.202051749 | Received 18 September 2020 | Revised 22 December 2020 | Accepted 12 January 2021 | Published online 23 February 2021

EMBO Reports (2021) 22: e51749

Introduction

Dynamic regulation of ubiquitination on proteins involved in DNA repair pathways is essential for proper functioning of these pathways. (De)-Ubiquitination enzymes that control these processes have gained a lot of attention, as these are attractive targets to attenuate DNA repair pathways. USP1 is a deubiquitinase (DUB) that acts on mono-ubiquitinated PCNA and FANCD2, making it crucial for the regulation of translesion synthesis and the Fanconi anaemia pathway, respectively (Nijman *et al*, 2005; Huang *et al*, 2006). Recently, it was also shown that USP1 inhibition resulted in replication fork destabilization and decreased viability of BRCA1-deficient cells indicating a synthetic lethal relationship (Lim *et al*, 2018). To target USP1 effectively, it would be important to know how its catalytic activity is regulated.

USP1 belongs to the ubiquitin-specific protease (USP) family of DUBs, and it forms a small sub-family with two other USPs, USP12 and USP46 (Mevissen & Komander, 2017). These USPs bind a common co-factor called UAF1 (also known as WDR48), which leads to activation of these enzymes by an increase in the catalytic turnover (k_{cat}) (Cohn *et al*, 2007, 2009). Relative to these paralogs, USP1 is much larger, primarily due to the presence of three inserts within its well-conserved USP catalytic domain (Figs 1A and EV1A). It also lacks the binding site for another activator, WDR20, which binds USP12 and USP46, leading to further activation (Kee *et al*, 2010). In contrast, it was reported recently that USP1 activity is further enhanced upon binding DNA and this interaction is mediated by insert L1 of USP1 (Lim *et al*, 2018). Insert L1 was also shown to be the site of multiple phosphorylations (Villamil *et al*, 2012; Olazabal-Herrero *et al*, 2015) and it has been reported to carry two nuclear localization signals that are important for its translocation to the nucleus (Garcia-Santisteban *et al*, 2012).

So far there is no structural information available for USP1 alone or the USP1-UAF1 complex, but crystal structures of the paralogs with and without the activators have been solved (Yin *et al*, 2015; Li *et al*, 2016; Dharadhar *et al*, 2016). Based on these USP12 and USP46 structures, it is clear that UAF1 binds USP1 on the "finger" sub-domain of the catalytic domain (Yin *et al*, 2015). It has also been shown that UAF1 activation of USP12 is mainly caused by a series of subtle structural rearrangements in various parts of the enzyme. One such region is the proximal knuckle (PK) helix and its preceding loop called the PK loop which also form a part of the WDR20 interface (Li *et al*, 2016). Interestingly, USP1 has a small insertion of 20 amino acids in the PK loop and this insert is located in the WDR20 binding interface of USP12 and USP46 (Insert L3, Fig EV1B). Whether this small insert of USP1 plays any role in its activation by UAF1 and if there are other unique elements within USP1 which compensate for the lack of WDR20 activation are not known.

USP1 activity on FANCD2-Ub is well studied and the N-terminal extension of USP1 is important for activity on FANCD2 (Arkinson *et al*, 2018). DNA binding was shown to promote USP1-UAF1 activity on FANCD2-Ub, but in this case, activation is dependent on a DNA-binding role of UAF1 (Liang *et al*, 2019). Additionally, the C-terminal SUMO-like domains (SLD) of UAF1 also play a role in the recruitment of USP1 to ubiquitinated substrates (Lee *et al*, 2010; Yang *et al*, 2011). In contrast, how USP1 acts on PCNA is not clear. Moreover, whether its activity is affected by DNA loading of PCNA-Ub has not been studied. This may be important for USP1 activity as

Division of Biochemistry and Oncode Institute, Netherlands Cancer Institute, Amsterdam, The Netherlands
*Corresponding author. Tel: +31 20 512 1959; E-mail: t.sixma@nki.nl

it is thought to travel along the replicating fork where it carries out its deubiquitinating activity in crucial DNA repair pathways (Dungrawala *et al*, 2015).

In this study, we demonstrate the molecular details of USP1 allosteric regulation by UAF1 and its natural substrate, i.e. DNA-loaded PCNA-Ub. We study the role of USP1 inserts on enzymatic

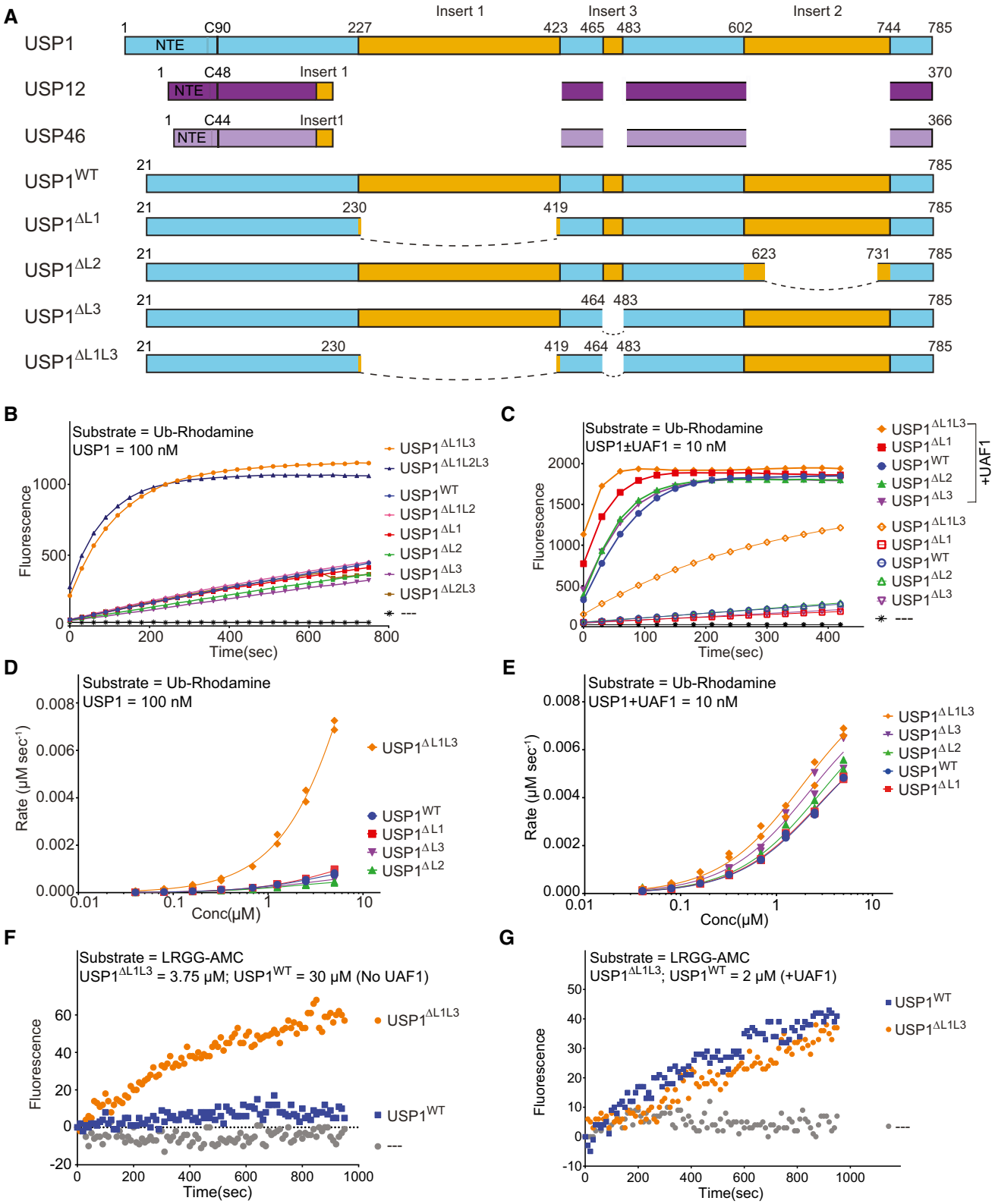

Figure 1.

Figure 1. UAF1 activates USP1 allosterically by relieving the insert 1 and insert 3 mediated auto-inhibition of USP1 catalytic activity.

A Schematic diagram of the USP1 sub-family and the USP1 deletion mutants tested in this study.
B Single point activity assays of $USP1^{WT}$ and deletion mutants on Ub-Rho show significantly increased activity in mutants where inserts L1 and L3 are both deleted.
C Single point activity assays of $USP1^{WT}$ and deletion mutants (±UAF1) on Ub-Rho show the loss in hyper-activation of $USP1^{\Delta L1L3}$ upon addition of UAF1.
D Michaelis–Menten analysis of USP1 deletion mutants against ubiquitin-rhodamine (Ub-Rho) shows that $USP1^{\Delta L1L3}$ has significantly higher activity compared to WT and other mutants ($n = 2$, biological replicates).
E Michaelis–Menten analysis of USP1 deletion mutants (+UAF1) against Ub-Rho shows that all deletions mutants have similar catalytic activity ($n = 2$, biological replicates).
F Comparing activity of $USP1^{WT}$ and $USP1^{\Delta L1L3}$ on a peptide substrate, i.e. LRGG-AMC (100 μM). $USP1^{\Delta L1L3}$ cleaves the peptide substrate more efficiently compared to $USP1^{WT}$ ($n = 2$, technical replicates).
G Comparing activity of $USP1^{WT}$ and $USP1^{\Delta L1L3}$ (+UAF1) on a peptide substrate, i.e. LRGG-AMC (100 μM). Addition of UAF1 allows cleavage of LRGG-AMC by both $USP1^{WT}$ and $USP1^{\Delta L1L3}$ ($n = 2$, technical replicates).

activity towards substrates of increasing complexity. This reveals that the combined action of inserts L1 and L3 inhibits USP1 catalytic activity and that this auto-inhibition is relieved by UAF1-dependent activation on a minimal substrate (Ub-Rho). On PCNA-Ub, we find that a PIP motif in insert L1 is crucial for activity. Finally, we developed a protocol to load PCNA-Ub on DNA. On this substrate, we identify a secondary enhancement in USP1 activity, that is only triggered upon interaction with DNA-loaded PCNA-Ub. Furthermore, we demonstrate that both DNA and PCNA interaction with USP1 are important for this substrate-mediated increase in activity.

Results and Discussion

USP1 catalytic activity is inhibited by its inserts

To address the role of the inserts in USP1 catalytic activity, we made deletion mutants of USP1 that either lack each insert individually or in combinations (Fig 1A). These deletion mutants were successfully purified and their catalytic activities were tested against the minimal substrate ubiquitin-rhodamine (Ub-Rho). None of the variants lacking a single insert ($USP1^{\Delta L1}$, $USP1^{\Delta L2}$, $USP1^{\Delta L3}$) showed any change in activity compared to wild-type USP1 ($USP1^{WT}$), but when both inserts L1 and L3 were removed ($USP1^{\Delta L1L3}$), a significant hyper-activation was observed (Fig 1B).

This hyper-activation was unique to this combination, as deletion of inserts L1 and L2 ($USP1^{\Delta L1L2}$) or insert L2 and L3 ($USP1^{\Delta L2L3}$) did not affect USP1 catalytic activity (Fig 1B). The insert L3 in USP1 is located in the PK loop. In USP12, this loop is important for activation, as mutation of a stretch of glycine residues within the loop leads to loss in activation of USP12 by either UAF1 or WDR20. In USP1, deletion of insert L3 alone does not affect USP1 activity but the deletion of both insert L3 and insert L1 leads to an increased activity of USP1.

We tested whether phosphorylation of serine 313 in insert L1 had a direct effect on USP1 catalytic activity, since Ser313 phosphorylation was previously reported as necessary for UAF1 binding and its ability to activate (Villamil *et al*, 2012; Olazabal-Herrero *et al*, 2015). We tested both the phospho-dead (Ser to Ala) and phosphomimic (Ser to Asp) mutations, but neither showed an effect on activity of USP1 alone or upon binding with UAF1, relative to $USP1^{WT}$ (Fig EV2A).

We performed Michaelis–Menten kinetic analysis under increasing concentrations of Ub-Rho substrate (Fig 1D, Table 1) and fitted $USP1^{WT}$ and all the deletion mutants. As the reaction velocity curves for $USP1^{\Delta L1L3}$ did not reach saturation, the estimation of Vmax and subsequently K_M was not reliable. To validate our findings, we fitted $USP1^{WT}$ and $USP1^{\Delta L1L3}$ activity data using *KinTek Explorer* (Johnson *et al*, 2009a) simultaneously, using all the data rather than initial rates only. Similar to our standard Michaelis–Menten analysis, this improved analysis again showed that the activation in $USP1^{\Delta L1L3}$ was mostly due to an increase in k_{cat} (Fig EV2B). We conclude that inserts L1 and L3 together inhibit the intrinsic catalytic activity of USP1.

UAF1 binding relieves insert L1- and insert L3-mediated auto-inhibition of USP1 activity

UAF1-mediated activation of USP1 is primarily due to an increase in k_{cat} (Cohn *et al*, 2007) which is similar to what we observe in $USP1^{\Delta L1L3}$. To test whether insert L1- and insert L3-mediated auto-inhibition of USP1 can be relieved by UAF1, we performed kinetic analysis in the presence of UAF1 on Ub-Rho (Fig 1E). We observed that the hyper-activation of USP1 that deletion of inserts L1 and L3 had caused was lost in the presence of UAF1, as the catalytic activity of $USP1^{\Delta L1L3}$ no longer differed significantly from $USP1^{WT}$, nor from any of the other deletion mutants (Fig 1C and E, Table 1). These experiments also show that the deletion of insert L1 and insert L3 is not sufficient to completely recapitulate UAF1-mediated activation as UAF1 binding can still activate $USP1^{\Delta L1L3}$. However, our data suggest that one of the primary mechanisms by which USP1 is activated by UAF1 is through relieving the auto-inhibition caused by the joint action of inserts L1 and L3.

Based on the published structures of USP12 + UAF1 and USP12 + UAF1 + WDR20 (Li *et al*, 2016; Dharadhar *et al*, 2016), we generated a homology model of USP1, that shows the location of the inserts of USP1 (Fig EV1B). Interestingly, insert L3 of USP1 overlaps with the binding site of WDR20 in USP12 suggesting that the effect of WDR20 could be mimicked by a joint mechanism which involves rearrangement of both inserts L1 and L3.

A defining feature of WDR20-dependent activation is that it is necessary for the ability of USP12 to cleave a peptide substrate, Leu-Arg-Gly-Gly (LRGG)-AMC, since USP12-UAF1 alone cannot cleave such a substrate (Li *et al*, 2016). Therefore, we analysed whether USP1 could process this substrate. First, we compared $USP1^{WT}$ in the presence and absence of UAF1. Like USP12, USP1 alone cannot cleave the peptide substrate. However, addition of UAF1 is sufficient to activate $USP1^{WT}$ such that it can now process this substrate (Fig 1 F and G), whereas USP12 requires WDR20 to make this happen (Fig EV2C; Li *et al*, 2016). Unlike $USP1^{WT}$, the $USP1^{\Delta L1L3}$ alone can

Table 1. Kinetic analysis of USP1^{WT} and deletion mutants using the Michaelis–Menten equation.

	(−UAF1)			(+UAF1)		
	k_{cat} (s^{-1})	K_M (μM)	k_{cat}/K_M (s^{-1} μM^{-1})	k_{cat} (s^{-1})	K_M (μM)	k_{cat}/K_M (s^{-1} μM^{-1})
USP1^{WT}	0.014 (±0.001)	3.80 (±0.52)	0.0036	0.73 (±0.03)	2.68 (±0.25)	0.272
USP1$^{\Delta L1}$	0.018 (±0.0007)	4.50 (±0.33)	0.0039	0.71 (±0.03)	2.53 (±0.23)	0.283
USP1$^{\Delta L2}$	0.004 (±0.0001)	1.03 (±0.11)	0.0043	0.80 (±0.03)	2.63 (±0.22)	0.306
USP1$^{\Delta L3}$	0.007 (±0.0003)	1.8 (±0.19)	0.0040	0.82 (±0.01)	2.03 (±0.09)	0.406
USP1$^{\Delta L1L3}$	0.26 (±0.01)	13.7 (±0.79)	0.019	1.01 (±0.07)	2.37 (±0.37)	0.425

cleave the peptide substrate which is in line with the idea that rearrangement of insert L1 brings about conformational changes in insert L3 which are necessary for activation of USP1 by bringing it to a WDR20-like state.

These results show on one hand that removal of insert L1- and insert L3-mediated auto-inhibition of USP1 brings it to a WDR20-bound-like state, and on the other hand that for USP1, the activation by UAF1 already achieves a state that requires WDR20 in the USP12/46 paralogs. It seems likely that this activation is mediated by some form of UAF1-induced conformational change in inserts L1 and L3. When UAF1 binds, at the tip of the finger sub-domain, this induces a cascade of rearrangements, as it does in USP12. We speculate that this brings about changes in insert L3, located at the base of the fingers and results in the removal of auto-inhibition by inserts L1 and L3 (Fig EV1B). To understand how L1 and L3 mediate their inhibition structural information will be important.

Insert L1 is necessary for USP1 activity on PCNA-Ub

To test whether the inserts of USP1 play any role in the deubiquitination of its natural substrate, i.e. mono-ubiquitinated PCNA (PCNA-Ub), we carried out activity assays on reconstituted PCNA-Ub (Hibbert & Sixma, 2012). In these assays, we used a TAMRA label at the N terminus of ubiquitin for ease of quantitation (Dharadhar *et al*, 2019), as this has no effect on the rates (Fig EV2D). Comparing WT and deletion mutants, we observed that loss of insert L1 in USP1 severely impairs its ability to deubiquitinate PCNA-Ub^{TAMRA} (Fig 2A), whereas this deletion does not affect activity on a minimal substrate.

We analysed the sequence of insert L1 in a multi-sequence alignment with different species (Fig 2B). We identified a degenerate PCNA-interacting-peptide (PIP) box, which is highly conserved across vertebrates (Fig 2B). Compared to traditional PIP motifs, there is one phenylalanine missing in the final FF, replaced by KF. Additionally, there was a possible APIM-like motif just upstream of the PIP site. We made two mutants, a triple mutant in the PIP (PIP1: I351A, L352A and F355A) and one with additional changes in the APIM (PIP2: I351A, L352A and F355A; W341A, L342A and K343A). These mutants were co-purified with UAF1 and tested for activity on PCNA-Ub^{TAMRA}. Both USP1^{PIP1} and USP1^{PIP2} had reduced activity on PCNA-Ub^{TAMRA} compared to USP1^{WT} but were not affected in their activity on a minimal substrate (Figs 2C and EV2E).

Importantly, we then analysed binding of USP1 to PCNA-Ub in a fluorescence polarization (FP) assay. Here we found that deletion of insert L1 (USP1$^{\Delta L1}$) or mutation of the PIP motif (PIP1) leads to a 10- and fivefold reduction in binding to PCNA-Ub^{TAMRA}, respectively (Fig 2D).

To validate the role of the PIP interaction between USP1 and PCNA, we made mutations in PCNA (PIM1: L126A and I128A; PIM2: D232A and P234A; PIM3: P253A and K254A), in the PIP interaction site (Eissenberg *et al*, 1997). USP1^{WT} activity was substantially reduced on the PCNA-Ub PIM1 and PIM2 mutant, while the activity on the PIM3 mutant was the same when compared to PCNA-Ub (WT) (Fig EV3A). We then compared the activity of USP1^{WT} and USP1^{PIP1} on both PCNA-Ub^{PIM1} and PCNA-Ub^{WT}. The activity of USP1^{WT} was reduced on PCNA-Ub^{PIM1} but activity of USP1^{PIP1} was not further depleted on PCNA-Ub^{PIM1} relative to PCNA-Ub^{WT}, indicating that both mutations affect the same interaction (Fig 2E and F). These binding and mutant data together confirm that insert L1 of USP1 contains a well-conserved PIP motif which is important for USP1 interaction and activity on PCNA-Ub.

Purification of PCNA-Ub loaded on circular DNA

USP1-UAF1 is known to play a role in PCNA-Ub-mediated translesion synthesis (Huang *et al*, 2006). Moreover, it has been suggested that USP1-UAF1 travels with elongating replication forks where it deubiquitinates its substrates. Removal of USP1 from this environment was shown to generate increased ubiquitination of proteins residing at the fork (Dungrawala *et al*, 2015). Other studies have shown that both USP1 and UAF1 have DNA-binding properties (Liang *et al*, 2016; Lim *et al*, 2018). We could confirm that USP1 binds DNA, and the fact that this interaction is dependent on insert L1 (Fig EV3B). However, we did not observe the (very small) effect on catalytic activity against a minimal substrate, Ub-rhodamine (Lim *et al*, 2018; Fig 3B). Nevertheless, we wondered if the observed interaction with DNA could affect the activity on a more natural substrate, PCNA-Ub loaded on DNA.

To enable analysis of USP1 activity on DNA-loaded substrate, we established efficient DNA loading procedures for human PCNA-Ub on circular DNA using the RFC clamp loader complex from yeast (Yoder & Burgers, 1991). First, we successfully purified PCNA-Ub where each monomer of the clamp was mono-ubiquitinated using previously published protocols (Hibbert & Sixma, 2012) and then we performed *in vitro* loading assays on nicked circular DNA (Fig 3A). Our results show that PCNA and PCNA-Ub are loaded with similar efficiency onto nicked circular DNA (Fig EV3C). We then used size exclusion chromatography to obtain large amounts of purified PCNA-Ub loaded on nicked circular DNA (Fig 3A). Due to the presence of a TAMRA label on each ubiquitin

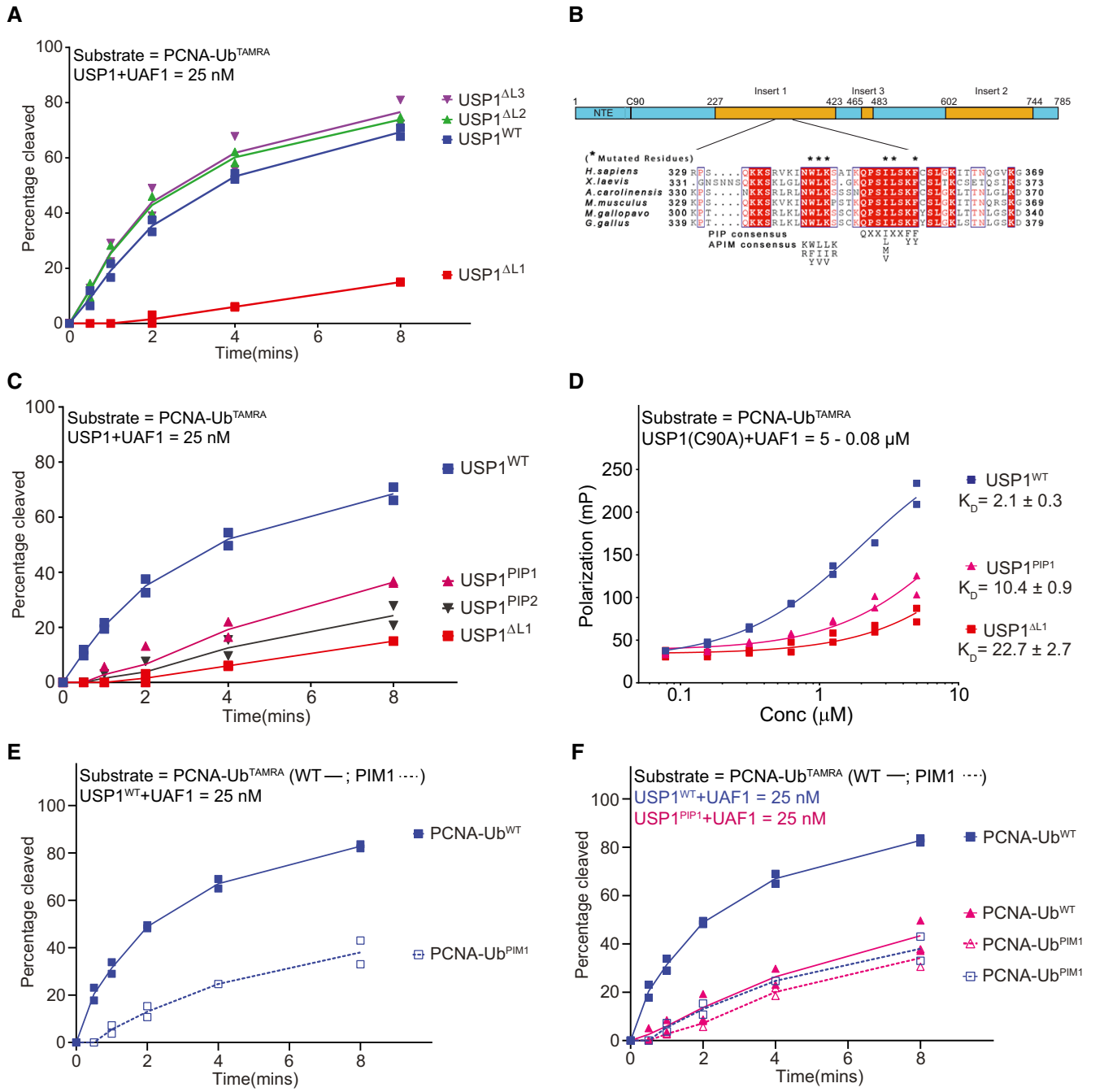

Figure 2. Insert L1 of USP1 contains a PIP motif which is essential for activity of USP1 on PCNA-Ub.

A Quantification of gel-based activity assays where the activity of USP1^{WT} and deletion mutants (+UAF1) on PCNA-Ub^{TAMRA} is compared. The USP1$^{\Delta L1}$ mutant has reduced activity on PCNA-Ub^{TAMRA} compared to the other USP1 variants tested (n = 2, biological replicates).

B Multiple sequence alignment of USP1 insert L1 which highlights the conservation of the PIP and APIM motif in USP1 across species, the residues mutated in this region are indicated with an asterisk.

C Quantification of gel-based activity assays where the activity of USP1 PIP mutants (+UAF1) on PCNA-Ub^{TAMRA} is compared. Both the PIP mutants have reduced activity on PCNA-Ub compared to USP1^{WT} (n = 2, biological replicates).

D FP-based binding assays of USP1 mutants (+UAF1) with PCNA-Ub^{TAMRA} show reduced binding of USP1$^{\Delta L1}$ and USP1^{PIP1} compared to USP1^{WT} (n = 2, technical replicates).

E Quantification of gel-based activity assays where the activity of USP1^{WT} + UAF1 on PCNA-Ub^{WT} is compared with PCNA-Ub^{PIM1} shows that PCNA-Ub^{WT} is cleaved much faster compared to PCNA-Ub^{PIM1} (n = 2, technical replicates (example shown here from 1 of 2 biological replicates)).

F Comparing activity of USP1^{WT} and USP1^{PIP1} (+UAF1) on PCNA-Ub^{WT} and PCNA-Ub^{PIM1} in gel-based assays shows that the activity of USP1^{WT} is severely reduced by the PIM1 mutation in PCNA, whereas USP1^{PIP1} activity is not further affected indicating that PIP1 and PIM mutation affect the same interaction (n = 2, technical replicates (example shown here from 1 of 2 biological replicates)).

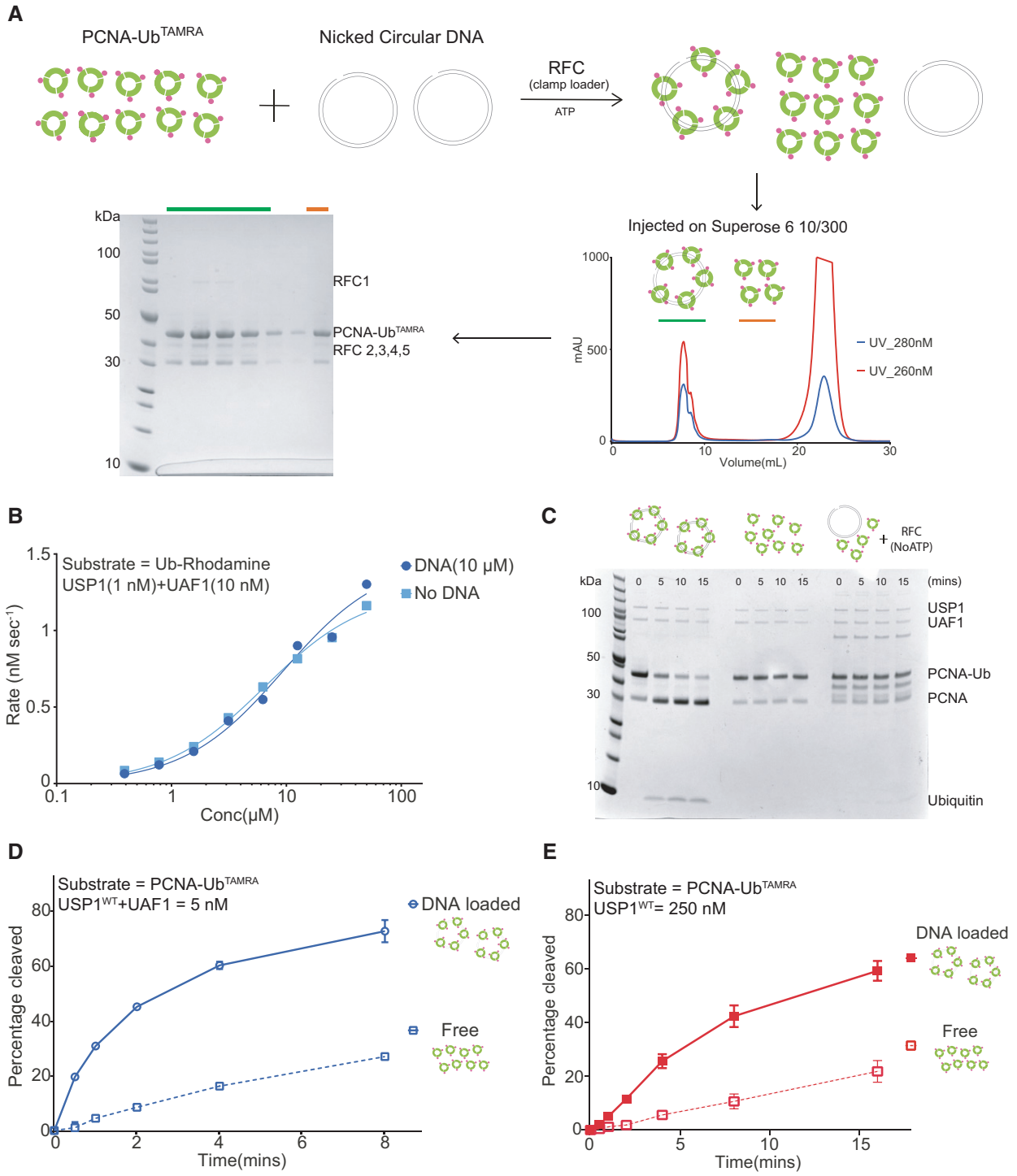

Figure 3. USP1 (±UAF1) has higher catalytic activity on PCNA-Ub when it is loaded on DNA.

A Schematic representation of loading and purification of PCNA-Ub on nicked circular DNA. The DNA-loaded PCNA-Ub elutes in the void of the SEC column, and this sample is collected and used for studying activity of USP1 on DNA-loaded PCNA-Ub.

B Michaelis–Menten analysis of USP1 + UAF1 with and without DNA (65 bp dsDNA) shows that DNA binding alone has no effect on USP1 activity ($n = 2$, technical replicates (example shown here from 1 of 2 biological replicates)).

C Coomassie-stained gel of *in vitro* activity assay showing increased activity of USP1-UAF1 on DNA-loaded PCNA-Ub compared to PCNA-Ub (−DNA) and PCNA-Ub (+DNA, +RFC and not ATP).

D Quantification of gel-based activity assays showing enhanced activity of USP1 + UAF1 on DNA-loaded PCNA-Ub compared to free PCNA-Ub ($n = 3$, technical replicates (example shown here from 1 of 2 biological replicates)).

E Quantification of gel-based activity assays showing enhanced activity of USP1 on DNA-loaded PCNA-Ub compared to free PCNA-Ub ($n = 3$, technical replicates (example shown here from 1 of 2 biological replicates)).

molecule, we could measure the exact concentrations of DNA-loaded PCNA-Ub which allowed us to perform quantitative *in vitro* deubiquitination assays.

The loading and purification of DNA-loaded PCNA-Ub is technically complex since many factors are involved in this reaction. Moreover, the half-life of PCNA on DNA is approximately 25 min which makes downstream experiments challenging due to the time constraints (Zhao *et al*, 2017). We circumvented this problem by carrying out the activity assays within 20 min after elution from a size exclusion column.

USP1 deubiquitinates PCNA-Ub more efficiently when it is loaded on DNA

We compared the deubiquitination activity of USP1 (±UAF1) on DNA-loaded PCNA-Ub with free PCNA-Ub in a gel-based activity assay. This showed that USP1-mediated ubiquitin hydrolysis is much faster when PCNA-Ub is loaded on DNA (Fig 3C–E). In these experiments, a minor fraction of the RFC co-eluted with DNA-loaded PCNA-Ub which allowed reloading of PCNA-Ub. However, this is not critical for the enhanced activity that we observe, as our control experiments with RFC and DNA in the absence of ATP do not show similar activity of USP1 (Fig 3C).

To obtain a detailed mechanism of USP1 activity, we performed kinetic analysis and modelling using the *KinTek explorer* software (Johnson *et al*, 2009a). We quantified USP1 (±UAF1) activity data under either different enzyme concentrations or different substrate concentrations against three different substrates, Ub-Rho, PCNA-Ub and DNA-loaded PCNA-Ub. We used SDS–PAGE-based setup for DNA-loaded PCNA-Ub and free PCNA-Ub (Figs 4A and EV4A). For PCNA-Ub, we additionally performed fluorescence polarization (FP)-based activity assays. Additionally, activity data of USP1 (±UAF1) on increasing concentrations of Ub-rhodamine were also included (Figs 4B and EV4B). The resulting data only fit in a model where the enhanced activity on DNA-loaded PCNA-Ub is mediated by an increase in affinity of USP1 (±UAF1) for the substrate with no change in catalytic activity (Figs 4C and EV4C). The *KinTek* analysis allowed us to quantify the magnitude of enhanced USP1 activity both in the presence and absence of UAF1. We observed that loading of PCNA increases USP1 activity ~2-fold, but in the presence of UAF1 the increase is fivefold (Fig 4C). The extra increase in USP1 activity given by UAF1 was caused by an increase in affinity for DNA-loaded PCNA-Ub of USP1 + UAF1, as the change is limited to K_M. This observation corresponds well with previously published data which show that UAF1 itself has DNA-binding properties in the range of 400 nM (Liang *et al*, 2019). To validate our kinetic modelling, we performed EMSA-based binding analysis for USP1 (±UAF1) on DNA which confirmed that USP1-UAF1 has stronger binding compared to USP1 alone (Fig EV4D). Altogether, our quantitative kinetic analysis shows that USP1 alone has enhanced activity on the natural substrate which is further strengthened when in complex with UAF1.

Insert L1 is critical for enhanced activity of USP1 on DNA-loaded PCNA-Ub

To dissect how USP1 has higher activity on DNA-loaded PCNA-Ub, we compared how insert deletions affected the activity on DNA-loaded PCNA-Ub relative to free (unloaded) PCNA-Ub. The $USP1^{\Delta L2}$ and $USP1^{\Delta L3}$ showed similar activity to $USP1^{WT}$ in cleaving PCNA-Ub by loading on DNA, but the $USP1^{\Delta L1}$ mutant showed no increase in activity on the loaded substrate (Fig 5A). The activity of $USP1^{\Delta L1}$ on PCNA-Ub is weak, and upon DNA loading its activity is not enhanced, in fact the activity is slightly lowered. These experiments show that the inserts L2 and L3 within USP1 are not involved in enhancing USP1 activity, while insert L1 is solely responsible for achieving this substrate-dependent increase in USP1 activity.

Since insert L1 has been previously shown to possess both PCNA- and DNA-binding properties, we tested if both these functions could be responsible for increased USP1 activity on DNA-loaded PCNA-Ub, relative to PCNA-Ub alone. To test how DNA binding could alter USP1 activity, we had to first identify residues involved in DNA binding so that we could separate the DNA- and PCNA-binding roles of insert L1. We analysed the insert L1 sequence using multiple sequence alignment and identified a region within insert L1 with several positively charged residues, which are well conserved across vertebrates (Fig 5B). Insert L1 WT and three sets of triple mutants containing charge swaps were cloned and then purified for DNA-binding studies using SPR. Our binding experiments showed that insert L1 can bind DNA, whereas all the triple mutants almost completely lost DNA binding (Fig 5B), thereby highlighting the role of electrostatic interaction in USP1 binding to DNA.

Insert L1-mediated DNA and PCNA interactions are crucial for increasing USP1 activity on DNA-loaded PCNA-Ub

Insert L1 of USP1 is a large insert of 200 amino acids with two distinct well-conserved regions for which we show interaction with DNA and PCNA, respectively. To gain further mechanistic insight into the insert L1-mediated increase of USP1 activity, we compared the activity of a USP1 DNA-binding mutant ($USP1^{DM1}$; KKK281EEE) and a USP1 PCNA interaction mutant ($USP1^{PIP1}$) on DNA-loaded PCNA-Ub with free PCNA-Ub. In both mutants, the increase in activity on the DNA-loaded substrate was substantially reduced relative to $USP1^{WT}$ (Fig 5C).

The $USP1^{DM1}$ mutant also has reduced activity on free PCNA-Ub compared to $USP1^{WT}$. This means that we cannot fully confirm whether its loss in activity on the DNA-loaded substrate is due to loss of DNA interaction. To delineate this further, we made a milder version ($USP1^{DM2}$, KKK281AEA) of the original DNA-binding mutant ($USP1^{DM1}$). The $USP1^{DM2}$ has similar activity on free PCNA-Ub as $USP1^{WT}$ but still lost DNA-binding ability when compared with $USP1^{WT}$ (Fig EV5A and B). When $USP1^{DM2}$ was tested on DNA-loaded, PCNA we found that it was poorly able to activate on this substrate, similar to $USP1^{DM1}$ (Fig EV5C). Taken together, these mutants confirm that DNA interaction through insert 1 is important for enhanced USP1 activity on DNA-loaded PCNA-Ub.

In contrast, the PCNA interaction mutant $USP1^{PIP1}$ had retained the ability to bind DNA, in an electrophoretic mobility shift assay (EMSA) on a 65 bp dsDNA (Fig 5D). This indicates that $USP1^{PIP1}$ is only affected in PCNA interaction and the loss of activity on DNA-loaded PCNA-Ub in this mutant is due to the defect in PCNA interaction.

Both the $USP1^{DM1}$ and $USP1^{PIP1}$ mutant still show considerable increase in activity on DNA-loaded PCNA-Ub, although to a lesser degree than $USP1^{WT}$. Therefore, we generated a USP1 double mutant lacking both DNA and PCNA interactions ($USP1^{PIP1+DM1}$)

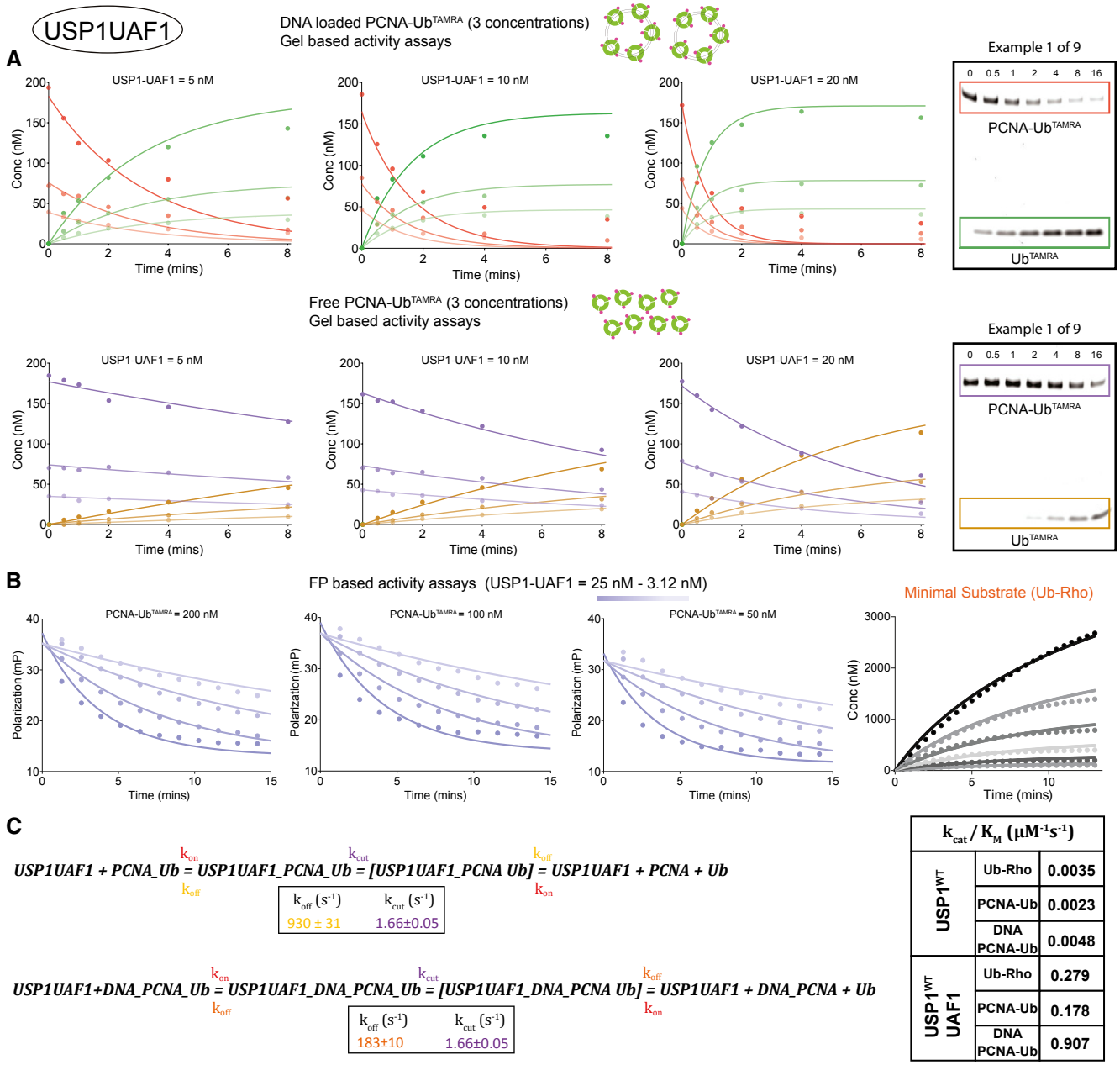

k_{cat}/K_M ($\mu M^{-1}s^{-1}$)		
$USP1^{WT}$	Ub-Rho	0.0035
	PCNA-Ub	0.0023
	DNA PCNA-Ub	0.0048
$USP1^{WT}$ UAF1	Ub-Rho	0.279
	PCNA-Ub	0.178
	DNA PCNA-Ub	0.907

Figure 4. Modelling the enhanced USP1 activity on DNA-loaded PCNA-Ub.

A Gel-based quantification of USP1-UAF1 activity on PCNA-Ub (DNA-loaded and free) for three different concentration of enzyme and substrate.

B FP-based activity assays on free PCNA-Ub (three concentrations of USP1 and PCNA-Ub) and activity of USP1 on increasing concentrations of Ub-Rho.

C Kinetic model of USP1-UAF1 activity on PCNA-Ub and DNA-loaded PCNA-Ub (Ub-Rho not shown here, see Fig EV4C for full model), constants with the same colour were linked during the fitting and they share same values.

Source data are available online for this figure.

and compared its activity on DNA-loaded PCNA-Ub and free PCNA-Ub. This double mutant has a very slightly enhanced activity on both substrates, but no significant difference between the two, indicating that it has completely lost the ability to enhance USP1 activity on DNA-loaded PCNA-Ub (Fig 5C). The complete loss of substrate-mediated activity increase in this USP1 mutant shows that PCNA interaction and DNA interaction together are necessary and sufficient for the increase in USP1 activity.

Altogether, these experiments establish insert L1 as a central regulatory hub for USP1 activity and highlight the role of various elements which play a role in allosteric regulation of USP1 activity. These mutations could be used for validation *in vivo*, but

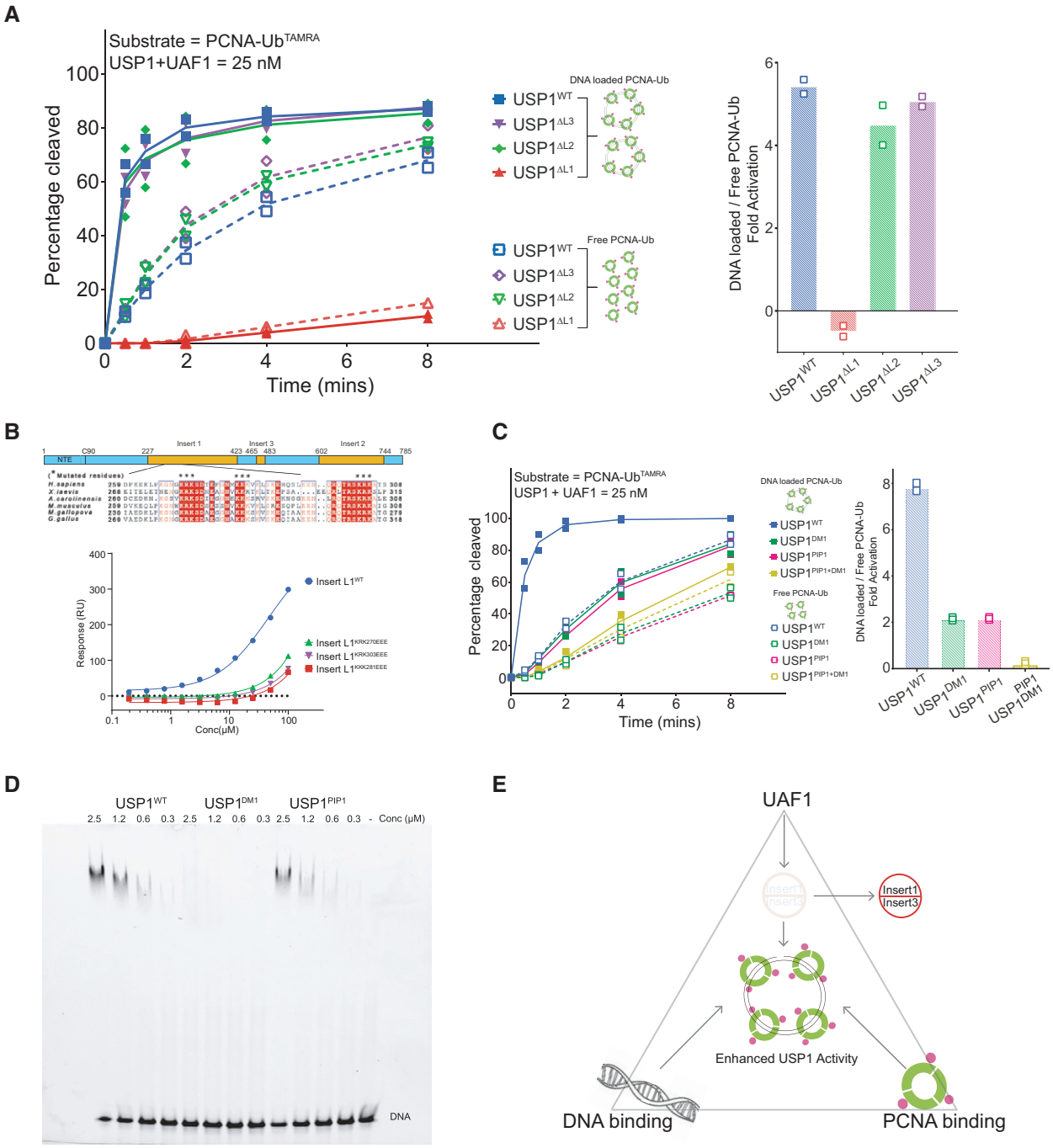

Figure 5. Insert L1-mediated DNA and PCNA interactions are crucial for increase in USP1 activity on DNA-loaded PCNA-Ub.

A Comparison of USP1^{WT} and deletion mutants (+UAF1) for activity on DNA-loaded PCNA-Ub (solid lines) and free PCNA-Ub (dashed lines) shows no increase in USP1$^{\Delta L1}$ activity on the loaded substrate. Left panel: Quantification of gel-based activity assays showing percentage of cleaved PCNA-Ub at the mentioned time points (n = 2, biological replicates). Right panel: Quantification of the activation fold observed in USP1^{WT} and mutants on DNA-loaded PCNA-Ub vs. free PCNA-Ub (n = 2, biological replicates).

B Multiple sequence alignment of USP1 insert L1 which highlights the DNA-binding region and the conservation of the positively charged residues across species. Three groups of positively charged residues (***) are mutated separately and tested for binding to double-stranded DNA (65 bp) using SPR which shows the importance of this region for DNA binding of USP1.

C Comparison of USP1^{DM1}, USP1^{PIP1} and USP1$^{PIP1+DM1}$ (+UAF1) activity on DNA-loaded PCNA-Ub (solid lines) and free PCNA-Ub (dashed lines) shows reduced increase in activity of these mutants compared to USP1^{WT}. Left panel: Quantification of gel-based activity assays showing percentage of cleaved PCNA-Ub at the mentioned time points (n = 2, technical replicates). Right panel: Quantification of the activation fold observed in USP1^{WT}, USP1^{PIP1}, USP1^{DM1} and USP1$^{PIP1+DM1}$ on DNA-loaded PCNA-Ub vs. free PCNA-Ub (n = 2, technical replicates).

D EMSA-based DNA-binding experiment shows that USP1^{PIP1} and USP1^{WT} have similar DNA-binding capability, while USP1^{DM1} has lost its ability to bind DNA.

E Schematic model for the role of insert L1 in USP1 activity regulation by UAF1 and DNA-loaded PCNA-Ub.

unfortunately the DNA-binding site overlaps with the previously assigned NLS, suggesting some difficulties in separating these functions out, Nevertheless, these newly identified USP1 hotspots are important as they may serve as novel starting points for development of specific allosteric modulators of USP1 function.

USP1 is activated by two distinct mechanisms involving UAF1 and DNA-loaded PCNA-Ub

The activation of USP1 by UAF1 takes place through an allosteric mechanism where the catalytic turnover (k_{cat}) of the enzyme is increased several fold (Cohn *et al*, 2007). We have shown here that this activation requires the rearrangement of inserts L1 and L3 which auto-inhibit USP1 in the absence of UAF1 (Fig 1D and E; Table 1). In this study, we also uncover a secondary step that enhances USP1 activity which is caused upon interaction with DNA-loaded PCNA-Ub.

Based on our preliminary biochemical analysis, we assumed that the increase in USP1 activity on DNA-loaded PCNA-Ub takes place solely through a change in the affinity of the enzyme for the loaded substrate vs. the unloaded substrate, as cleavage rate values remained similar in individual runs. Therefore, they were linked in the final analysis accordingly (Fig EV4, Table 2).

Interestingly, we note that not only USP1-UAF1 is activated by DNA loading of PCNA, but also USP1 alone, which shows an increase in catalytic efficiency of from 2.3 mM^{-1} s^{-1} to 4.8 mM^{-1} s^{-1}. This confirms that also in the absence of UAF1, USP1 has higher activity on the DNA-loaded substrate. The PCNA and DNA interaction regions of insert L1 are likely to play a key role in this since we have shown that mutating these two regions leads to no increase in activity.

Nevertheless, the increase in activity is larger in the presence of UAF1, increasing from 178 mM^{-1} s^{-1} on PCNA-Ub to 907 mM^{-1} s^{-1} on DNA-loaded PCNA-Ub (Table 2, Fig 4C), primarily due to a difference in K_{off}. In both USP1 and USP1-UAF1, the enzyme is faster on DNA-loaded PCNA-Ub, but the increase in activity due to DNA loading is higher in the presence of UAF1: fivefold increase in USP1-UAF1 and a twofold increase in USP1 alone (Table 2, Fig 4C).

Recently, it has been shown that USP1 activity on Ub-FANCD2 is higher in the presence of DNA and this is dependent on UAF1 binding (Liang *et al*, 2019). This suggests that the DNA interaction of UAF1 may help to increase the affinity of USP1 for DNA-loaded PCNA-Ub (Figs 4 and EV4). Apparently, USP1 activity is regulated by two separate mechanisms, one which involves the change in catalytic turnover upon UAF1 binding, while the other involves a change in affinity towards its natural substrate, i.e. DNA-loaded PCNA-Ub (Fig 5E). Therefore, we propose that UAF1 activation and DNA-loaded PCNA-Ub-mediated enhancement of USP1 activity are mechanistically independent of each other.

Materials and Methods

Plasmids and cloning

Human USP1 and UAF1 (WDR48) constructs were obtained from Martin Cohn (University of Oxford). Human WDR20 (isoform 5) was subcloned from the HAP1 cell line (Essletzbichler *et al*, 2014) into pGEXNKI-GST3C-LIC vector (Luna-Vargas *et al*, 2011) for expression in *Escherichia coli*. Plasmid pBL481 for overexpression of the entire RFC complex was a gift from Peter Burgers (Washington University, St. Louis). A 1.7 Kb circular plasmid (RC1766) used for PCNA-Ub loading was a gift from Rafael Fernández Leiro (CNIO, Madrid). The USP1 constructs were all cloned in the pFastbac-HTb vector (N-terminal His tag), with a G670A + G671A mutation to prevent autocleavage of the USP1 protein (Huang *et al*, 2006). The UAF1 construct was cloned into the pFastbac1 vector (N-terminal Strep tag) for expression in *Spodoptera frugiperda* (*sf*9) cells. USP1 point mutants were generated using QuikChange site-directed mutagenesis, and mutants were confirmed by sequencing. The AEA mutant of USP1 contains an additional M583I cloning mutation. USP1 insert 1 (230–420) was cloned into the pGEXNKI-GST3C-LIC vector, and the ^{Cys}Ubiquitin construct was cloned into the pETNKI-His-SUMO2-kan vector for expression in *E. coli* (Luna-Vargas *et al*, 2011). Plasmids used for PCNA, Uba1 (E1), UbCH5C (S22R), ubiquitin have been described previously (Hibbert & Sixma, 2012).

Protein expression and purification

Complexes of recombinant UAF1 with USP1 wild-type and mutant proteins (USP1^{KKK281EEE}, USP1^{PIP1,2}, USP1 insert deletions) were co-expressed and co-purified from *sf*9 cells as described previously (Dharadhar *et al*, 2019). Complex of USP12-UAF1 protein was co-expressed and co-purified from *sf*9 cells as described previously (Dharadhar *et al*, 2016). PCNA, UBA1, ubiquitin and UbCH5c (S22R) (UBE2D3) were expressed and purified from *E. coli* as described previously (Hibbert & Sixma, 2012).

Table 2. *KinTek* modelling of USP1 (±UAF1) activity on three substrates, i.e. Ub-Rho, PCNA-Ub and DNA-loaded PCNA-Ub.

		−UAF1			+UAF1		
	Units	Ub-Rho	PCNA-Ub	DNA-PCNA-Ub	Ub-Rho	PCNA-Ub	DNA-PCNA-Ub
k_{on}[a]	μM^{-1} s^{-1}	100^{α}	100^{α}	100^{α}	100^{α}	100^{α}	100^{α}
k_{off}[a]	s^{-1}	$594 \pm 24^{\beta}$	$930 \pm 31^{\gamma}$	433 ± 8	$594 \pm 24^{\beta}$	$930 \pm 31^{\gamma}$	183 ± 10
k_{cat} (k_{cut})[a,b]	s^{-1}	$0.021 \pm 0.001^{\delta}$	$0.021 \pm 0.001^{\delta}$	$0.021 \pm 0.001^{\delta}$	$1.66 \pm 0.05^{\epsilon}$	$1.66 \pm 0.05^{\epsilon}$	$1.66 \pm 0.05^{\epsilon}$
K_M	μM	5.94 ± 0.24	9.3 ± 0.31	4.33 ± 0.08	5.94 ± 0.24	9.3 ± 0.31	1.83 ± 0.01
k_{cat}/K_M	μM^{-1} s^{-1}	0.0035 ± 0.0002	0.0023 ± 0.0001	0.0048 ± 0.0002	0.279 ± 0.014	0.178 ± 0.008	0.907 ± 0.027

[a]Constants with the same symbol (α, β, γ, δ) were linked during the fitting, and they share same values.
[b]Although k_{cut} mathematically is not equivalent to Michaelis–Menten catalytic rate constant k_{cat}, the difference in the values between them in this model is neglectable in comparison to measurement and fitting errors.

Purification of USP1

In experiments where USP1 was used without UAF1, both USP1 wild-type and deletion mutants were expressed by Baculovirus expression in *sf*9 cells for 72 h by infecting cells at a density of 1×10^6 cells ml^{-1}. Cells were harvested in lysis buffer (50 mM Tris pH 8.0, 200 mM NaCl, 5 mM TCEP) with complete EDTA-free protease inhibitor (Sigma) and lysed by sonication. The lysed cells were spun down (53,000 × *g* for 30 min) in a high-speed centrifuge at 4°C, and the supernatant was loaded on a column of Ni^{2+}-Sepharose beads pre-equilibrated in lysis buffer. Once the supernatant had passed through the column, it was washed with 30 column volumes (CV) of wash buffer (lysis buffer + 20 mM Imidazole pH 8.0) and then USP1 was eluted with 5CV of elution buffer (lysis buffer + 500 mM Imidazole pH 8.0). The elution fraction was diluted twofold with 50 mM Tris pH 8.0 and loaded on an anion exchange column (Resource Q, GE Healthcare) pre-equilibrated with 50 mM Tris pH 8.0, 100 mM NaCl, 2 mM DTT (IEX buffer). The column was washed with 3CV of IEX buffer and elution was carried out by applying a salt gradient of 20CV from 100 mM to 1 M NaCl. Fractions containing USP1 were combined and concentrated at 4°C in an Amicon Ultra-15 centrifugal filter unit (30 kDa cut-off; Merck) and then loaded on a size exclusion column (Superdex 200 10/300; GE) equilibrated in 20 mM HEPES pH 7.5, 150 mM NaCl, 2 mM DTT (SEC buffer). Pure USP1 fractions were concentrated at 4°C and stored at −80°C.

Purification of USP1 insert L1

Insert L1 wild-type and mutant proteins were expressed in BL21 (*E. coli*) cells by inducing cells at an OD of 0.8 with 0.2 mM IPTG followed by overnight expression at 18°C. Cells were harvested in lysis buffer (50 mM Tris pH 8.0, 200 mM NaCl, 2 mM DTT) with complete EDTA-free protease inhibitor (Sigma) and lysed by sonication. The lysed cells were spun down (53,000 × *g* for 30 min) in a high-speed centrifuge at 4°C, and the lysate was loaded on a column of Glutathione Sepharose 4B beads (GE Healthcare) pre-equilibrated in lysis buffer. Once the lysate had passed through the column, it was washed with 30CV of lysis buffer following which insert 1 was eluted with 5CV of elution buffer (lysis buffer + 50 mM reduced glutathione). GST-tag was cleaved in 2 h with 3°C protease while dialysing against 20 mM Tris pH 8.0, 100 mM NaCl, 2 mM DTT (Heparin buffer). The sample was collected from the dialysis bag and loaded on a Heparin column (GE Healthcare) pre-equilibrated in Heparin buffer. After sample application, the column was washed with 3CV of Heparin buffer and protein was eluted using a salt gradient of 20CV from 100 mM to 1 M NaCl. Fractions containing pure insert 1 were combined and concentrated at 4°C in an Amicon Ultra-15 centrifugal filter unit (10 kDa cut-off; Merck) and then loaded on a size exclusion column (Superdex 200 10/300; GE) equilibrated in SEC buffer. Pure insert 1 fractions were concentrated at 4°C and stored at −80°C.

Purification of GST-WDR20

GST-WDR20 was expressed in BL21 (*E. coli*) cells by inducing at an OD of 0.8 with 0.2 mM IPTG followed by overnight expression at 18°C. Cells were harvested in lysis buffer (50 mM Tris pH 7.5, 200 mM NaCl, 2 mM DTT) with complete EDTA-free protease inhibitor (Sigma) and lysed by sonication. The lysed cells were spun down (53,000 × *g* for 30 min), and the clarified lysate was loaded on a column of Glutathione Sepharose 4B beads (GE Healthcare) pre-equilibrated in lysis buffer. The beads were incubated with the lysate for 30 min at 4°C, and then, the lysate was allowed to pass through the column. The beads were washed with 30CV of lysis buffer, and GST-WDR20 was eluted in 5CV of lysis buffer with 20 mM reduced glutathione. The eluted sample was then loaded on a cation exchange column (POROS S, GE Healthcare) pre-equilibrated with 20 mM Tris pH 7.5, 200 mM NaCl, 2 mM DTT (IEX buffer). GST-WDR20 eluted upon applying a salt gradient of 10CV from 200 to 1,000 mM NaCl. Fractions containing GST-WDR20 were combined and concentrated at 4°C in an Amicon Ultra-15 centrifugal filter unit (30 kDa cut-off; Merck).

Purification of PCNA-Ub^{TAMRA}

Ubiquitin with a cysteine residue introduced at the N terminus after the methionine at position 1 (^{Cys}Ubiquitin) was labelled using maleimide linked TAMRA dye (Setareh Biotech). The purification of ^{Cys}Ubiquitin and its labelling with maleimide linked TAMRA has been described previously (Dharadhar *et al*, 2019).

The components required for the *in vitro* mono-ubiquitination of PCNA are Ub^{TAMRA}, Uba1, PCNA and UbCH5c (S22R) (UBE2D3). Once all the components were purified, the reaction was setup as described previously to a final reaction volume of 20 ml (Hibbert & Sixma, 2012). Upon completion of the reaction, the PCNA-Ub^{TAMRA} was purified from the rest of the components using anion exchange chromatography followed by size exclusion chromatography in GF buffer. The purified sample was concentrated at 4°C in an Amicon Ultra-15 centrifugal filter unit (10 kDa cut-off; Merck) and stored at −80°C.

Purification of RFC

The procedure for the purification of the RFC complex was adapted from a previously described protocol by the Burgers laboratory (Gomes *et al*, 2000). Protein was expressed in *E. coli* grown in Terrific broth (TB) medium. Cells were induced at an OD of 1.6 with 0.2 mM IPTG followed by overnight expression at 16°C. The cells were harvested in lysis buffer (30 mM HEPES 7.5, 200 mM NaCl, 1 mM DTT, 0.5 mM EDTA, 10% Glycerol, 0.5 mM PMSF, complete protease inhibitor) and lysed by sonication. The lysed cells were kept stirring on ice and 0.5% Polymin P was added followed by incubation for 5 min. The lysed cells were spun down at 53,000 × *g* for 40 min at 4°C, and the supernatant was collected. Ammonium sulphate (0.28 g ml^{-1}) was added to the supernatant while stirring on ice for 30 min and then the precipitated proteins were collected by spinning at 12,000 × *g* for 60 min. The proteins were resuspended in 30 mM HEPES 7.5, 1 mM DTT, 0.5 mM EDTA, 10% Glycerol, 0.5 mM PMSF, complete protease inhibitor followed by dialysis for 2 h against 30 mM HEPES 7.5, 100 mM NaCl, 1 mM DTT, 0.5 mM EDTA, 10% Glycerol. The dialysed sample was loaded on a cation exchange column (POROS S 6 ml, GE Healthcare) pre-equilibrated in 30 mM HEPES 7.5, 100 mM NaCl, 1 mM TCEP, 10% Glycerol (PorosS buffer). Subsequently, the column was washed with 5CV of PorosS buffer and the protein was eluted by applying a

salt gradient from 100 mM to 1 M NaCl. The fractions containing all five subunits of RFC are collected and loaded on Ni^{2+}-Sepharose beads pre-equilibrated in 20 mM HEPES 7.5, 200 mM NaCl, 10% Glycerol, 1 mM TCEP (His buffer). The column is then washed with 30CV of wash buffer (His buffer + 20 mM Imidazole pH 8.0), and the protein is eluted with 5CV of elution buffer (20 mM HEPES pH 7.5, 300 mM NaCl, 300 mM Imidazole pH 8.0, 10% Glycerol, 1 mM TCEP, 0.05% Ampholytes). Sample was concentrated at 4°C in an Amicon Ultra-15 centrifugal filter unit (10 kDa cut-off; Merck) and then loaded on a size exclusion column (Superdex 200 10/300; GE) equilibrated in 20 mM HEPES pH 7.5, 200 mM NaCl, 10% Glycerol, 1 mM DTT, 0.05% Ampholytes. Fractions containing the RFC complex were concentrated at 4°C and stored at −80°C.

Production of nicked circular DNA

The RC1766 plasmid was nicked using a nicking endonuclease, Nt.BbvCI. The nicked circular DNA was then loaded on a size exclusion column (Superose 6 10/300; GE) equilibrated in 20 mM HEPES pH 7.5, 150 mM NaCl, 2 mM DTT. The fractions containing the nicked circular DNA were collected and concentrated in an Amicon Ultra-15 centrifugal filter unit (10 kDa cut-off; Merck) up to a final concentration of 1 μM.

Purification of DNA-loaded PCNA-Ub

To load PCNA-Ub on DNA, we added 10 μM PCNA-Ub, 0.2 μM nicked circular DNA and 1 μM RFC in 20 mM HEPES pH 7.5, 150 mM NaCl, 10 mM $MgCl_2$, 2 mM ATP, 1 mM DTT at a final volume of 500 μl. The reaction was incubated at 4°C for 2 h and then it was injected on a size exclusion column (Superose 6 10/300; GE) pre-equilibrated in 20 mM HEPES pH 7.5, 100 mM NaCl, 10 mM $MgCl_2$, 0.5 mM ATP, 1 mM DTT. DNA-loaded PCNA-Ub elutes at the void volume of the column and is ready to be used for downstream applications.

Ub-rhodamine activity assays

Enzymatic activity was followed as release of fluorescent rhodamine from the quenched Ub-rhodamine substrate (UbiQ; The Netherlands), providing a direct readout for DUB activity. The fluorescence intensity at 590 nm was measured using the Pherastar plate reader (BMG LABTECH GmbH, Germany). The assays were carried out in 384-well plates (Corning, flat bottom, low flange) at 25°C in a reaction buffer of 20 mM HEPES pH 7.5, 150 mM NaCl, 5 mM DTT, 0.05% Tween-20. Single point assays were carried out at 1 μM substrate concentration and different enzyme concentrations. The enzyme concentrations used are indicated in the figure. For the Michaelis–Menten analysis, 100 nM of USP1 and 10 nM of USP1-UAF1 were used against different substrate concentration starting from 5 to 0.1 μM. The initial velocity rates were obtained from the slopes of the linear phase of the curve. These rates were plotted against substrate concentration and fitted with a Michaelis–Menten model using non-linear regression in GraphPad Prism 7 software (GraphPad Software Inc., USA). Since the reaction velocity of $USP1^{L1L3}$ has not reached saturation, the K_M values obtained by this approach are unreliable. Therefore, the $USP1^{\Delta L1L3}$ activity curves were fitted in addition using Kintek Explorer version 8.0 (Kintek Corporation (Johnson *et al*, 2009a)) alongside $USP1^{WT}$ to establish if there is indeed a real change in the K_M values between the two enzymes.

Peptide substrate LRGG-AMC activity studies

Enzymatic activity was followed as a release of fluorescent AMC from the quenched LRGG-AMC substrate (Boston Biochem), providing a direct readout for DUB activity on a minimal peptide. The fluorescence intensity at 440 nm was measured using the Pherastar plate reader (BMG LABTECH GmbH, Germany). The assays were carried out in 384-well plates (Corning, flat bottom, low flange) at 25°C in a reaction buffer of 20 mM HEPES pH 7.5, 150 mM NaCl, 5 mM DTT, 0.05% Tween-20. USP1 WT and mutants were tested at different concentrations against 100 μM of LRGG-AMC, and enzyme concentrations used are indicated in the figures.

Fluorescence polarization-based binding assay

The FP assays were carried out in 384-well plates at 25°C in a reaction buffer of 20 mM HEPES pH 7.5, 100 mM NaCl, 2 mM DTT, 0.05% Tween-20. All USP1-UAF1 mutants tested also had their active site cysteine mutated to alanine which resulted in catalytically dead USP1-UAF1. These mutants were tested for binding to PCNA-Ub^{TAMRA} by measuring FP at varying concentrations of USP1-UAF1 (5 μM–80 nM) while keeping the PCNA-Ub^{TAMRA} at a constant concentration of 25 nM. The FP measurements were taken in the Pherastar plate reader (BMG LABTECH GmbH, Germany), using excitation wavelength of 540 nm (±20), and the polarization was detected at 590 nm (±20). The initial polarization of PCNA-Ub^{TAMRA} was set at 30 mp, and any increase in polarization upon binding of USP1-UAF1 was plotted using GraphPad Prism 7 (GraphPad software Inc., USA).

SPR-based binding assay

SPR binding experiments were carried out in the Biacore T200 system (GE, USA) to test the binding of USP1 WT and mutants with double-stranded DNA. The running buffer used for the SPR experiment was 20 mM HEPES pH 7.5, 150 mM NaCl, 2 mM DTT, 0.05% Tween-20, 1 mg ml^{-1} BSA and the DNA was immobilized on a Streptavidin chip (Sensor chip SA, GE) using the biotin present on the 5′ end of the DNA. The binding experiments were carried out in the single cycle kinetics mode with 10 sequential injections of USP1 and $USP1^{\Delta L1}$ from 25 to 0.05 μM, while the insert 1 and mutants were injected from 100 to 0.2 μM. Data from a reference flow cell (−DNA) which was run in parallel to the experiment were subtracted from the signal using the Biacore T200 evaluation software. The final analysis and figures were done in GraphPad Prism 7 software (GraphPad Software Inc, USA).

Electrophoretic mobility shift assays

USP1 binding to DNA was also tested by performing EMSAs with native 4–12% pre-cast Tris-Glycine gels at 4°C (Life Technologies). The gels were equilibrated by running them in Tris-Glycine buffer at 125 V for 90 min at 4°C prior to the start of the actual experiment. USP1 and mutants were serially diluted to make a twofold dilution series from 2.5 to 0.3 μM, and the DNA was added to a final

concentration of 0.2 μM. The USP1-DNA samples were incubated at 4°C for 15 min prior to loading in the pre-equilibrated gel which was then run at 125 V for 90 min at 4°C. DNA bands were visualized by GelRed staining followed by imaging in a ChemiDoc XRS instrument (Bio-Rad).

Gel-based activity assays

PCNA-Ub^{TAMRA} cleavage assays were performed in a reaction buffer composed of 20 mM HEPES pH 7.5, 100 mM NaCl, 5 mM $MgCl_2$, 0.25 mM ATP, 2 mM DTT. The cleavage reaction was started by addition of USP1 (±UAF1) followed by incubation at room temperature for the specified time course. The concentration of DUB used for the kinetic modelling experiments was 1, 0.5, 0.25 μM for USP1 and 20, 10, 5 nM for USP1-UAF1. All the mutants tested for activity on PCNA-Ub^{TAMRA} were in complex with UAF1, and they were run in parallel with wild-type USP1 at a concentration of 25 nM. Samples were collected at the indicated time points, and the reaction was stopped by adding SDS loading buffer. Samples were loaded on NuPAGE 4–12% Bis-Tris SDS gel (Invitrogen) and separated by running them at 180 V for 30 min. The TAMRA fluorescence signal was visualized using a Typhoon FLA-9500 gel scanner (GE Healthcare), and the concentration of PCNA-Ub^{TAMRA} and ubiquitin was quantified by comparing the TAMRA fluorescence of the individual bands with a calibration curve of TAMRA fluorescence in the same experimental setting.

Kinetic modelling of USP1 activity on DNA-loaded and free PCNA-Ub

Kintek Explorer version 8.0 (Kintek Corporation (Johnson *et al*, 2009a)) was used to fit the reaction mechanism. Cleavage data from three different substrates, i.e. Ub-rhodamine, PCNA-Ub and DNA-loaded PCNA (Figs 4 and EV4), were used for the fitting simultaneously. The fitting presented here is based on all the data, but the model was built in stages. At first step, enzymatic activity assay data of USP1 and USP1-UAF1 on minimal substrate Ub-rhodamine were fitted to a product inhibition model, which includes three steps: substrate binding, substrate cleavage and product release. The association rate constants of substrate and product binding (k_{on}) were set to diffusion limit approximation (100 $\mu M^{-1}\ s^{-1}$), and dissociation rate constants substrate and product (k_{off}) share the same value in both reactions. The results of the fitting (k_{cat}, K_M and k_{cat}/K_M) were compared with the results of Michaelis–Menten calculations (Table 1).

$$k_{cat} = \frac{k_{cut} * k_{off}}{k_{cut} + k_{off}}$$

$$K_M = \frac{k_{off}}{k_{on}}$$

$$k_{cat}/K_M = \frac{k_{cut} * k_{on}}{k_{cut} + k_{off}}$$

k_{cut}—cleavage rate constant;
k_{on}—substrate and product binding rate constant;
k_{off}—substrate and product dissociation rate constant

Next, the enzymatic activity FP assay data on PCNA-Ub^{TAMRA} substrate were added to the analysis. Same model was used and in addition to previous constrains cleavage rate constant (k_{cut}) was shared same value for each enzyme, and k_{off} shared same value in the reactions with same substrate. In addition, concentrations of enzymes and substrates were allowed to vary up to 5% from the theoretical value in order to compensate for experimental pipetting error. At the last step of model building, the data from gel-based enzymatic activity assays on PCNA-Ub^{TAMRA} and DNA-loaded PCNA-Ub^{TAMRA} substrates were added to the analysis. Same model and rate constraints were used for the fitting. However, it was not possible to achieve good global fit of the date unless the value of k_{off} for USP1 in reaction with DNA-loaded PCNA-Ub^{TAMRA} was different from the value of k_{off} for USP1-UAF1 in reaction with DNA-loaded PCNA-Ub^{TAMRA}. Solution landscape analysis of the fitted parameters was done using FitSpace Editor (Johnson *et al*, 2009b). It showed correlation between values of k_{off} and k_{cut}. Thus, only their ratios and magnitude are directly defined within the model, meaning that the values of kinetic efficiency (k_{cat}/K_M) are giving the best representation of the modelling results.

Data availability

This study includes no data deposited in external repositories.

Expanded View for this article is available online.

Acknowledgements
We thank Niels Keizer and Andrea Murachelli for critical reading of the manuscript and other group members for their helpful suggestions. We thank Peter Burgers for the RFC construct and Martin Cohn for USP1 and UAF1 constructs. We thank Athanassios Adamopoulos for help with mutant cloning. We thank Farid El Oualid for providing us with Ub-rhodamine. The authors acknowledge funding from the Dutch Cancer Society (KWF 2014-6858) and Oncode Institute.

Author contributions
SD designed, performed and analysed biochemical experiments with assistance from TKS and AF. SD and SS performed mutant design and cloning. SD, SS and WJvD performed protein purification. Kinetic modelling using the KinTek software was done by AF. SPR experiments were done by SD and AF. TKS conceived and coordinated the study, and SD wrote the paper with assistance from TKS. All authors reviewed the results and approved the final version of the manuscript.

Conflict of interest
The authors declare that they have no conflict of interest.

References

Arkinson C, Chaugule VK, Toth R, Walden H (2018) Specificity for deubiquitination of monoubiquitinated FANCD2 is driven by the N-terminus of USP1. *Life Sci Alliance* 1: 1–15

Cohn MA, Kowal P, Yang K, Haas W, Huang TT, Gygi SP, D'Andrea AD (2007) A UAF1-containing multisubunit protein complex regulates the fanconi anemia pathway. *Mol Cell* 28: 786–797

Cohn MA, Kee Y, Haas W, Gygi SP, D'Andrea AD (2009) UAF1 is a subunit of multiple deubiquitinating enzyme complexes. *J Biol Chem* 284: 5343–5351

Dharadhar S, Clerici M, Van DWJ, Fish A, Sixma TK (2016) A conserved two-step binding for the UAF1 regulator to the USP12 deubiquitinating enzyme. *J Struct Biol* 196: 437–447

Dharadhar S, Kim RQ, Uckelmann M, Sixma TK (2019) *Quantitative analysis of USP activity in vitro*, 1st edn, Amsterdam: Elsevier Inc.

Dungrawala H, Rose KL, Bhat KP, Mohni KN, Glick GG, Couch FB, Cortez D (2015) The replication checkpoint prevents two types of fork collapse without regulating replisome stability. *Mol Cell* 59: 998–1010

Eissenberg JC, Ayyagari R, Gomes XV, Burgers PM (1997) Mutations in yeast proliferating cell nuclear antigen define distinct sites for interaction with DNA polymerase delta and DNA polymerase epsilon. *Mol Cell Biol* 17: 6367–6378

Essletzbichler P, Konopka T, Santoro F, Chen D, Gapp BV, Kralovics R, Brummelkamp TR, Nijman SMB, Bürckstümmer T (2014) Megabase-scale deletion using CRISPR/Cas9 to generate a fully haploid human cell line. *Genome Res* 24: 2059–2065

Garcia-Santisteban I, Zorroza K, Rodriguez JA (2012) Two nuclear localization signals in USP1 mediate nuclear import of the USP1/UAF1 complex. *PLoS One* 7: e38570

Gomes XV, Gary SL, Burgers PMJ (2000) Overproduction in *Escherichia coli* and characterization of yeast replication factor C lacking the ligase homology domain. *J Biol Chem* 275: 14541–14549

Hibbert RG, Sixma TK (2012) Intrinsic flexibility of ubiquitin on proliferating cell nuclear antigen (PCNA) in translesion synthesis. *J Biol Chem* 287: 39216–39223

Huang TT, Nijman SMB, Mirchandani KD, Galardy PJ, Cohn MA, Haas W, Gygi SP, Ploegh HL, Bernards R, D'Andrea AD (2006) Regulation of monoubiquitinated PCNA by DUB autocleavage. *Nat Cell Biol* 8: 339–347

Johnson KA, Simpson ZB, Blom T (2009a) Global Kinetic Explorer: a new computer program for dynamic simulation and fitting of kinetic data. *Anal Biochem* 387: 20–29

Johnson KA, Simpson ZB, Blom T (2009b) FitSpace Explorer: an algorithm to evaluate multidimensional parameter space in fitting kinetic data. *Anal Biochem* 387: 30–41

Kee Y, Yang K, Cohn MA, Haas W, Gygi SP, D'Andrea AD (2010) WDR20 regulates activity of the USP12.UAF1 deubiquitinating enzyme complex. *J Biol Chem* 285: 11252–11257

Lee KY, Yang K, Cohn MA, Sikdar N, D'Andrea AD, Myung K (2010) Human ELG1 regulates the level of ubiquitinated proliferating cell nuclear antigen (PCNA) through its interactions with PCNA and USP1. *J Biol Chem* 285: 10362–10369

Li H, Lim KS, Kim H, Hinds TR, Jo U, Mao H, Weller CE, Sun J, Chatterjee C, D'Andrea AD *et al* (2016) Allosteric activation of ubiquitin-specific proteases by β-propeller proteins UAF1 and WDR20. *Mol Cell* 63: 249–260

Liang F, Longerich S, Miller AS, Tang C, Buzovetsky O, Xiong Y, Maranon DG, Wiese C, Kupfer GM, Sung P (2016) Promotion of RAD51-mediated homologous DNA pairing by the RAD51AP1-UAF1 complex. *Cell Rep* 15: 2118–2126

Liang F, Miller AS, Longerich S, Tang C, Maranon D, Williamson EA, Hromas R, Wiese C, Kupfer GM, Sung P (2019) DNA requirement in FANCD2 deubiquitination by USP1-UAF1-RAD51AP1 in the *Fanconi anemia* DNA damage response. *Nat Commun* 10: 1–8

Lim KS, Li H, Roberts EA, Gaudiano EF, Clairmont C, Sambel LA, Ponnienselvan K, Liu JC, Yang C, Kozono D *et al* (2018) USP1 Is required for replication fork protection in BRCA1-deficient tumors. *Mol Cell* 72: 925–941.e4

Luna-Vargas MPA, Christodoulou E, Alfieri A, van Dijk WJ, Stadnik M, Hibbert RG, Sahtoe DD, Clerici M, De MV, Littler D *et al* (2011) Enabling high-throughput ligation-independent cloning and protein expression for the family of ubiquitin specific proteases. *J Struct Biol* 175: 113–119

Mevissen TET, Komander D (2017) Mechanisms of deubiquitinase specificity and regulation. *Annu Rev Biochem* 86: 159–192

Nijman SMB, Huang TT, Dirac AMG, Brummelkamp TR, Kerkhoven RM, D'Andrea AD, Bernards R (2005) The deubiquitinating enzyme USP1 regulates the fanconi anemia pathway. *Mol Cell* 17: 331–339

Olazabal-Herrero A, García-Santisteban I, Rodríguez JA (2015) Structure-function analysis of USP1: insights into the role of Ser313 phosphorylation site and the effect of cancer-associated mutations on autocleavage. *Mol Cancer* 14: 33

Villamil MA, Liang Q, Chen J, Choi YS, Hou S, Lee KH, Zhuang Z (2012) Serine phosphorylation is critical for the activation of ubiquitin-specific protease 1 and its interaction with WD40-repeat protein UAF1. *Biochemistry* 51: 9112–9113

Yang K, Moldovan GL, Vinciguerra P, Murai J, Takeda S, D'Andrea AD (2011) Regulation of the *Fanconi anemia* pathway by a SUMO-like delivery network. *Genes Dev* 25: 1847–1858

Yin J, Schoeffler AJ, Wickliffe K, Newton K, Starovasnik MA, Dueber EC, Harris SF (2015) Structural insights into WD-repeat 48 activation of ubiquitin-specific protease 46. *Structure* 23: 2043–2054

Yoder BL, Burgers PMJ (1991) *Saccharomyces cerevisiae* replication factor C: I. purification and characterization of its atpase activity. *J Biol Chem* 266: 22689–22697

Zhao G, Gleave ES, Lamers MH (2017) Single-molecule studies contrast ordered DNA replication with stochastics translesion synthesis. *Elife* 6: e32177